Wu *et al. Molecular Cancer* (2024) 23:184
https://doi.org/10.1186/s12943-024-02099-4

Molecular Cancer

RESEARCH Open Access

LAMTOR1 decreased exosomal PD-L1 to enhance immunotherapy efficacy in non-small cell lung cancer

Bo Wu[1], Xin Huang[2], Xiang Shi[3], Meixi Jiang[4], Hongxu Liu[3*] and Li Zhao[1*]

Abstract

Great progress has been made in utilizing immune checkpoint blockade (ICB) for the treatment of non-small-cell lung cancer (NSCLC). Therapies targeting programmed cell death protein 1 (PD-1) and its ligand PD-L1, expressed on tumor cells, have demonstrated potential in improving patient survival rates. An unresolved issue involves immune suppression induced by exosomal PD-L1 within the tumor microenvironment (TME), particularly regarding $CD8^+$ T cells. Our study unveiled the crucial involvement of LAMTOR1 in suppressing the exosomes of PD-L1 and promoting $CD8^+$ T cell infiltration in NSCLC. Through its interaction with HRS, LAMTOR1 facilitates PD-L1 lysosomal degradation, thereby reducing exosomal PD-L1 release. Notably, the ability of LAMTOR1 to promote PD-L1 lysosomal degradation relies on a specific ubiquitination site and an HRS binding sequence. The findings suggest that employing LAMTOR1 to construct peptides could serve as a promising strategy for bolstering the efficacy of immunotherapy in NSCLC. The discovery and comprehension of how LAMTOR1 inhibits the release of exosomal PD-L1 offer insights into potential therapeutic strategies for improving immunotherapy. It is imperative to conduct further research and clinical trials to investigate the feasibility and efficacy of targeting LAMTOR1 in NSCLC treatment.

Keywords LAMTOR1, Exosomes, PD-L1, Non-small cell lung cancer, Immunotherapy

Introduction

In recent research, there has been an increasing emphasis on immune checkpoint blockade (ICB) therapy. One intriguing mechanism involves inhibiting PD-L1 to protect tumor cells from immune surveillance by $CD8^+$ T cells [1, 2]. PD-L1 interacts with the PD-1 receptor on T cells' surface, suppressing the anti-tumor functions of $CD8^+$ T cells and aiding in evading the immune system [3–5]. Emerging studies indicate that using PD-L1 inhibitors yields significant clinical benefits in treating various cancers, such as non-small cell lung cancer (NSCLC) [6–9]. While current antibody agents effectively inhibit PD-L1 on cancer cells' outer membrane, the presence of exosomal PD-L1 underscores the importance of focusing on the tumor microenvironment (TME) [10]. HRS, a

*Correspondence:
Hongxu Liu
hgjxlzdsb@163.com
Li Zhao
sjhxnhzl@163.com
[1]Department of Pulmonary and Critical Care Medicine, Shengjing Hospital of China Medical University, Shenyang 110136, China
[2]Department of General practice medicine, Shengjing Hospital of China Medical University, Shenyang 110022, China
[3]Department of Thoracic Surgery, Cancer Hospital of China Medical University, Liaoning Cancer Hospital & Institute, Shenyang 110042, China
[4]Department of Neurology, The Fourth Affiliated Hospital, China Medical University, Shenyang 110032, China

component of the ESCRT complex, controls the release of exosomal PD-L1, restricting $CD8^+$ T cell infiltration in the TME [11, 12]. Therefore, comprehending the molecular regulation of exosomal PD-L1 could be a vital element in strategies aimed at enhancing anti-tumor immunity.

LAMTOR1 functions as an anchor, regulating lysosomal trafficking through its interaction with the Ragulator complex (p14/LAMTOR2, MP1/LAMTOR3, HBXIP, and C7orf59). This complex engages with RagAB/CD GTPase and V-ATPase, thereby activating mammalian target of rapamycin complex 1 (mTORC1) associated cellular functions on the lysosomal surface [13–15]. Activated by this Ragulator complex, mTORC1 oversees cellular biosynthesis, energy metabolism, autophagy, cellular growth, and lysosomal maturation [16–19]. The N-terminal ubiquitination site within the unstructured domain of LAMTOR1 facilitates autophagy by limiting its interaction with vacuolar H^+-ATPase [19]. With its position on the late endosomal and lysosomal, LAMTOR1 emerges as a central hub for the regulation of intracellular signaling pathways [17]. Understanding the natural regulators of PD-L1 lysosomal degradation can considerably facilitate the evolution and fine-tuning of targeting strategies, thereby ameliorating the outcomes of NSCLC immunotherapy. In our research, we demonstrated that LAMTOR1 promotes PD-L1 lysosomal degradation via its interaction with HRS, consequently limiting the release of exosomal PD-L1. This activity critically depends on the ubiquitination site and an HRS binding sequence. Leveraging this knowledge, we crafted a LAMTOR1 peptide that targets PD-L1 for lysosomal degradation. LAMTOR1 peptide also significantly enhanced the therapeutic efficacy of anti-PD-1. LAMTOR1 peptide combined with anti-PD-1 immunotherapy promotes tumor infiltration of $CD8^+$ T cells. Therefore, this study illustrates the efficacy of LAMTOR1 peptide as a mode of cancer immunotherapy.

Method

Patients and tissues

From November 2019 to January 2022, the surgical division of the Cancer Hospital of China Medical University harvested 85 human NSCLC tumor samples. NSCLC tissues were histologically confirmed for each patient. The study excluded patients with infections, inflammatory diseases, or those who underwent neoadjuvant treatment. The patients underwent staging based on the guidelines of the American Joint Committee on Cancer version 8 (AJCC 8). Samples were obtained after obtaining consent from the patients, and the research protocols were sanctioned by the Ethical Review Committee of China Medical University, adhering to all ethical regulations pertaining to research involving human participants. Blood samples were collected from healthy donors after receiving approval from the Ethical Review Committee of China Medical University. Written consent was obtained from each donor prior to the collection of blood. All experiments involving these blood samples were carried out in accordance with relevant ethical guidelines.

Cell lines and reagents

The human non-small cell lung cancer (NSCLC) cell lines employed in this study include H3122, H520, A549, H1650, H1299, HCC366, HCC827, H460, H1975, H358, Calu-1, H820, H1573 and H2009 [20], along with a mouse lung cancer cell line (LLC). These were procured from the American Type Culture Collection (ATCC) and verified using short tandem repeat (STR) analysis. Post-acquisition, H460, H1975, Calu-1 and H820 cells were cultivated in RPMI-1640 medium (Corning), supplemented with 10% fetal bovine serum (FBS) from BI, 1% penicillin and streptomycin from Gibco. The H3122, H520, A549, H1650, H1299, HCC366, HCC827, H358, H1573, H2009 and LLC cells were nourished in DMEM (Corning), with 10% FBS from BI, 1% penicillin, and streptomycin from Gibco. All cell lines were incubated at 37℃ within a 5% CO2 environment. The reagents used were: Bafilomycin A1 (Baf-A1) (catalog #HY-100558; MedChemExpress).

Cell transfection

Lung cancer cells lines were transfected with short hairpin RNA (shRNAs) for knockdown human *LAMTOR1* (*sh-LAMTOR1: 5′*-CCCATCCCGTTCTCTGATTTG-*3′*) through lentiviral systemic culture. We also targeted the expressions of human *HRS* (*sh-HRS: 5′*-GCACGTCTTTCCAGAATTCAA-*3′*), human *RAB7a* (*si-RAB7a: 5′*-AGGCTAGTCACAATGCA-*GATA-3′*), and human *ATG7* (*si-ATG7: 5′*-CTGCTGAGGAGCTCTCCAT-*3′*) using lentiviral transfection. To establish stably transfected cell lines, we employed puromycin (2 μg/mL) post-transfection.

Plasmid construction

The expression vectors encoding GFP-LAMTOR1, HA-HRS, HA-PD-L1, and GFP-PD-L1 were created by integrating synthetically produced cDNA that encoded the tags and LAMTOR1, HRS, and PD-L1 into the vectors via the EcoRI/NotI MCS. In addition, EcoRI/NotI sites were utilized to insert cDNA strands encoding specific peptides. Through the replacement of synthesized sequences of N-terminal or C-terminal-deleted LAMTOR1 fragments with the full-length complementary DNA of LAMTOR1 between the EcoRI and NotI sites of the GFP-LAMTOR1 plasmid, various constructs such as GFP-LAMTOR1-ΔN1-3 (20–78), ΔN1-2 (20–60), ΔN1 (20–31), ΔN2 (31–60), ΔN3 (60–78), and ΔC (144–161) were prepared. Furthermore, GFP-LAMTOR1-ΔK20,

GFP-LAMTOR1-ΔK31, and GFP-LAMTOR1-ΔK60 mutants with K-R alterations were derived from GFP-LAMTOR1. By inserting cDNA strands encoding HA tags and specified peptide segments (S1, S2, S3) into the pEGFP-C1 vector using the EcoRI/NotI MCS, GFP chimeric proteins were generated. Chimeric proteins with GFP were synthesized by incorporating cDNA fragments that encode HA tags and designated peptide portions (S1, S2, S3) into the pEGFP-C1 vector via the EcoRI/NotI MCS. Sequencing of the prepared plasmids was conducted to confirm the planned mutations and eliminate any unintended changes. Verification of the updated relative molecular weights of the expressed proteins was achieved through western blot analysis.

Purification of the extracellular vesicles

Exosomes secreted by cells were obtained from cell supernatant by incubating the cells in a medium supplemented with 10% exosome-depleted FBS. Standard differential centrifugation was utilized to purify extracellular vesicles from the supernatants of cell cultures maintained for 48 to 72 h. To eliminate cell debris and dead cells, cell culture supernatants underwent centrifugation at 2000 g for 20 min. Following centrifugation at 17,000 g for 40 min, the microvesicles were reconstituted. The resultant supernatant underwent ultracentrifugation at 100,000 g for 2 h at 4℃. The residual material was resuspended in PBS before undergoing a final ultracentrifugation cycle at 100,000 g for another 2 h.

Isolation of exosomes by sucrose gradient centrifugation

The extraction of exosomes through sucrose gradient density centrifugation was executed following the protocols delineated in relevant, preceding studies [21]. The exosomes that were procured by means of differential ultracentrifugation underwent a high-speed centrifugation process at 100,000 g for a span of 2.5 h. Subsequent to collection, these exosomes were submerged individually in sucrose solutions of varying densities, specifically 10–16%, 22–28%, 34–40%, 46–52%, 58–64%, and 70–82%. Each fraction therein was diluted in the ratio 1:100, and re-suspended at 100,000 g, followed by another round of centrifugation for 2.5 h in PBS, prior to undertaking western blot. Qualitative analysis of these samples was realized using western blot, and corroborated further with a western blot technique that employed exosome protein antibodies.

ELISA

Detecting exosomal PD-L1 was achieved by using 0.3 μg/well (100 μl) of anti-PD-L1 (clone 5H1-A3) monoclonal antibody, which was immobilized on an ELISA plate (96 wells) and incubated overnight at 4 °C (Biolegend). Subsequent cell blocking was performed using 200 μl of blocking buffer (Pierce) for one hour at room temperature. Exosome samples were isolated from cell culture supernatant using a serial dilution technique and then subjected to overnight incubation at 4 °C. Each well was treated with biotinylated PD-L1 antibody (clone MIH1, eBioscience) and incubated at 25 °C for 1 h. Following this, a 100 μl solution of streptavidin for horseradish peroxidase conjugation (BD Biosciences), diluted in PBS with 0.5% BSA, was added to each well and incubated at 25 °C for an additional hour. Standard curves were generated using recombinant PD-L1 protein (R&D Systems, Cat# 156-B7) and recombinant P-selectin protein (R&D Systems, Cat# 137-PS). The detection of IL-2 (BioLegend, Cat#589106), IFN-γ (BioLegend, Cat#502504), and TNF-α (BioLegend, Cat#430207) expressing $CD8^+$ T cells followed the same procedure.

Characterization of the purified exosomes

To ascertain the size distribution of exosomes, an initial step of diluting the exosomes tenfold using a 0.22 μm filter membrane is essential to gain an optimal observation count. Post dilution, 30 μl of diluted exosomes are applied onto a carbon-coated copper mesh that is positioned atop a sealed membrane, allowed to settle for between 2 and 5 min. Consequently, the supporting membrane is left to dry after being stained with a uranium acetate dye solution for a duration of 90 s. The stained support membrane is then placed on filter paper to dry for a subsequent 3 h in preparation for observation. Ultimately, size measurement and separation of exosomes are performed utilizing the NanoSight NS300 instrument (Malvern Instruments LTD), with the database being analyzed through NTA software (NTA version 2.3).

Immunohistochemistry (IHC)

Immunohistochemistry (IHC) staining was conducted on paraffin-embedded tissues using antibodies targeting LAMTOR1/C11orf59 (CST, Rabbit mAb, #8975) and PD-L1 (28−8) (Abcam, Rabbit mAb, ab205921), PD-L1 (D5V3B) (CST, Rabbit mAb, #64988). The protein expression patterns were assessed based on established protocols. The staining results were evaluated through the H-score (Histochemistry score), calculated by multiplying the positivity rate of cells by the staining intensity. A H-score median value of 150 was designated as the threshold for categorizing NSCLC tissues into either "low expression" or "high expression" groups. Approval for all procedures involving human samples was obtained from the Institutional Review Board of China Medical University, with informed consent acquired from all participants.

GST pull down and mass spectrometry (LC-MS/MS)

Purification of GST marking the bait protein expression (GST-LAMTOR1), the use of immobilized affinity ligand combines the bait protein and solid substrate stability, then the bait protein and cell lysis liquid mixed under test incubation. In this process, the bait protein interaction with the target protein and together, which cleaning without specific combination of proteins. The target proteins interacting with the decoy protein was obtained, and then identification of the tested protein was performed through Liquid Chromatography-Mass Spectrometry-Mass Spectrometry (LC-MS/MS). Progenesis QI software from Waters Corporation was employed for LC-MS/MS analysis on the basis of public databases (www.hmdb.ca/, https://www.lipidmaps.org/). Differentially expressed genes (DEGs) were later enriched into Kyoto Encyclopedia of Genes and Genomes (KEGG) pathways and Gene Ontology (GO) functions with R software.

Western blot

Total cellular protein or exosomal protein (10–40 μg) was extracted using sodium dodecyl sulfate-polyacrylamide gel electrophoresis (SDS-PAGE), after which it was transferred onto a polyvinylidene fluoride (PVDF) membrane (Millipore, Billerica, MA, USA). Follow-on steps comprised the addition of Bovine Serum Albumin (BSA) for membrane blocking, after which an overnight incubation took place with the targeted antibody, kept at a temperature of 4℃.

Primary antibodies: LAMTOR1/C11orf59(D11H6) (CST, Rabbit mAb, #8975); PD-L1 (E1L3N®) (CST, XP® Rabbit mAb, #13684); HRS (D7T5N) (CST, Rabbit mAb, #15087); CD63 (GeneTex, Mouse mAb, GTX28219); TSG101 (E6V1X) (CST, Rabbit mAb, #72312); Alix (E6P9B) (CST, Rabbit mAb, #92880); GAPDH (D16H11) (CST, XP® Rabbit mAb, #5174).

Real-time PCR

mRNA levels was achieved using real-time PCR. The extraction of RNA was accomplished by applying TRIzol Reagent (Invitrogen), which was subsequently converted into cDNA with the help of the StepOne Real-Time PCR System (BioRad, 1708840). The resulting data were processed using StepOne Software v2.2.1 (Bio-Rad). Analyses were performed in triplicates for each sample, with GAPDH acting as the normalization reference.

The following primers were used:

IFN-γ F: GCATTCCAGTTGCTGCCTACT R: ACCAGGCATGAGAAGAAATGCT
TNF-α F: GCTTCGCCGTCTCCTACCA R: TTGGCAAGGGCTCTTGATG
IL-2 F: CCTCAACTCCTGCCACAATGT R: TGCGACAAGTACAAGCGTCAGT
GAPDH F: AACTCCCTCAAGATTGTCAGCAA R: CATGGATGACTTTGGCTAGAGGA

Isolation and stimulation of peripheral blood mononuclear cells (PBMCs)

Blood samples were procured from a cohort of 45 healthy donors post-approval by the Ethical Review Committee of China Medical University. Each donor provided written consent before the blood collection process commenced. All subsequent experiments involving these blood specimens were conducted in compliance with the pertinent ethical guidelines. Subsequent to isolation using a ficoll gradient and storage following standard procedures, the separation of Peripheral blood mononuclear cells (PBMCs) was performed. Human PBMC-derived $CD8^+$ T cells were sorted through flow cytometry techniques for purification. The activation of $CD8^+$ T cells was accomplished by utilizing anti-CD3/CD28 beads (CST, #70976) for a duration of 24 h under conditions of 37℃ and 5% CO_2.

Treatment of CD8+ T cells co-cultured with exosomal PD-L1

$CD8^+$ T cells from human blood mononuclear cells (PBMCs) were purified by flow cytometry sorting. In the $CD8^+$ T cell proliferation experiment, 2×10^5 $CD8^+$ T cells were first incubated with 20 μL CFSE (diluted 1:500) (CST, #72782) at 37 °C for 25 min. Subsequently, anti-CD3/CD28 beads (CST, #70976) and exosomes isolated from treated 2×10^7 NSCLC cells (H1975 and H358) were added to the $CD8^+$ T cells for co-cultivation over a 3-day period under conditions of 37 °C and 5% CO_2. In the $CD8^+$ T cell cytotoxicity experiment, anti-CD3/CD28 beads (CST, #70976) and exosomes isolated from treated 2×10^7 NSCLC cells (H1975 and H358) were first added to the 2×10^5 $CD8^+$ T cells for co-cultivation over a 3-day period. Subsequently, Granzyme B (GzmB) (CST, #65563) was incubated $CD8^+$ T cells at 37 °C for 30 min. After the above co-cultivation treatment, collect $CD8^+$ T cells and conduct flow cytometry analysis to evaluate their characteristics. A FACS Calibur (BD Biosciences, USA) was employed for flow cytometry. Subsequently, after cell analysis, Cell Quest software (BD Biosciences, USA) was employed to calculate results. The expression levels of IL-2, IFN-γ, and TNF-α in $CD8^+$ T cells were measured through the consistent co-culture system outlined earlier, employing ELISA and RT-PCR methodologies.

Immunofluorescence staining

Plasmid transfection into cells was carried out using Lipofectamine 3000 for a duration of 48 h. After cell

fixed, permeabilization with 0.1% Triton X-100, and blocking with a 5% BSA buffer for 30 min. The fixed cells were then subjected to incubation with the primary antibody against, maintained at 4 ℃ overnight, followed by a two-hour incubation with a fluorescence-conjugated secondary antibody. The resulting fluorescence was visualized using a Nikon confocal microscope at a 60× magnification. Following this, the immunofluorescence co-localization results in all cells were quantitatively analyzed using Image-Pro Plus (IPP) 6.0 software (Media Cybernetics, Rockville, MD, USA). The methodology consisted of opening the co-localization image, accessing the "Measure" tab, setting the parameters to "Co-localization," and progressing by clicking "Forward." This procedure produced a scatter plot correlating the intensities of the red and green channels, and calculated the Pearson correlation coefficient for subsequent statistical analysis.

Primary antibodies: LAMTOR1/C11orf59 (CST, Rabbit mAb, #8975); PD-L1 (CAL10) (Abcam, Mouse mAb, ab279293); PD-L1 (28−8) (Abcam, Rabbit mAb, ab205921); HRS (HGS) (Proteintech, Mouse mAb, 67818-1-Ig); CD63 (GeneTex, Mouse mAb, GTX28219); TSG101 (Proteintech, Mouse mAb, 67381-1-Ig); Rab7a (E9O7E) (CST, Mouse mAb, #95746); ATG7 (Proteintech, Mouse mAb, 67341-1-Ig); LAMP1 (D4O1S) (CST, Mouse mAb, #15665).

Co-immunoprecipitation

Protein-protein interaction was detected through immunoprecipitation, using the method previously described [22]. Co-immunoprecipitation (Co-IP) was employed to discern protein interactions. Plasmid transfection into lung cancer cells was performed using Lipofectamine 3000 over a 48 h period. The transfected cells were lysed with a RIPA buffer that contained a blend of protease and phosphatase inhibitors. Primary antibodies were integrated into the lysate flasks and spun overnight at 4℃. The concoction of cleavage products and antibodies was then added to magnetic beads and rotated for 50 min at 25℃. Following this, the plates were cleaned three times with 200μL PBS at room temperature, each cleaning spin lasting for 10 min. The mix for western blot experiments was achieved by boiled 35μL SDS sample buffer at 95℃ for 10 min and a brief centrifugation at 4500 r.p.m for 30 s.

Primary antibodies: LAMTOR1/C11orf59(D11H6) (CST, Rabbit mAb, #8975); HRS (D7T5N) (CST, Rabbit mAb, #15087); PD-L1 (E1L3N®) (CST, XP® Rabbit mAb, #13684); GFP (GeneTex, Mouse mAb, GTX628528); GFP (GeneTex, Rabbit mAb, GTX113617); HA tag (GeneTex, Mouse mAb, GTX628489); HA tag (GeneTex, Rabbit mAb, GTX115044-01); GAPDH (D16H11) (CST, XP® Rabbit mAb, #5174).

Secondary antibodies: Mouse Anti-rabbit IgG (Conformation Specific) (L27A9) mAb (HRP Conjugate) #5127.

LAMTOR1 peptide synthesis, purification and labeling

The peptide sequences were synthesized utilizing Fmoc solid-phase methodology on a 2-chlorotrityl chloride (2CTC) resin, followed by purification via reverse-phase high-performance liquid chromatography (RPHPLC) to validate their accurate mass as well as purity of ≥95% through LC-MS. The labeling of peptide sequences was accomplished by generating an amide linkage with the side chain of a singular lysine residue employing Alexa Fluor® 488 (A488). For labeling the desiccated peptide (~0.5 mg), it was dissolved in 75 μl of N, N-dimethylformamide (DMF), combined with 25 μl of A488 sulfo-2,6-dichlorobenzothiazole (Life Technologies, #A30052), and 2 μl of N, N-diisopropylethylamine (DIPEA). The labeled peptide fragments were subsequently purified, and their mass and purity were validated. The concentration of these peptide fragments in the solution was ascertained by measuring the absorbance at 280 nm.

In vivo mice study

Pathogen-free C57BL/6 mice were obtained and kept at the China Medical University's animal facility. Inoculation of LCC cells and LCC/PD-L1 cells (overexpressing PD-L1 of LCC cells) (1×10^6 cells in 100 μl medium) into the subcutaneous of 8-week-old C57BL/6 mice resulted in the formation of subcutaneous tumors, which were given treatment of control group (Exosome of LCC cells); OE-PD-L1 group (Exosome of LCC/PD-L1 cells) or LAMTOR1 peptide on every 3 days. The mice were euthanized either 30 days post cell inoculation or before 30 days once the longest tumor dimension reached 1.0 cm. We utilized digital caliper measurements to calculate the tumor volume based on the ellipsoid model (with the formula: $V = W(\text{width})^2 \times L(\text{length})/2$.

Pathogen-free C57BL/6 mice were obtained and kept at the China Medical University's animal facility. Inoculation of LCC/PD-L1 cells (1×10^6 cells in 100 μl medium) into the tail vein of 8-week-old C57BL/6 mice resulted in the formation of tumors, which were given treatment of Control; anti-PD-1; LAMTOR1 peptide; or LAMTOR1 peptide+anti-PD-1. Tumor measurements were captured through the utilization of the IVIS Lumina II imaging system (PerkinElmer), concomitantly employing hematoxylin and eosin (H&E) staining staining to investigate the potential side effects of co-administering LAMTOR1 peptide with immunotherapy. The study was conducted following guidelines set forth by the Ethical Review of Research Committee of China Medical University.

Statistics

Statistical analysis and graph compilation were performed using SPSS 22.0 and GraphPad Prism 9.3 software. All experiments were independently performed in triplicates. The Mann-Whitney U test or t-test was utilized for comparison of measurement data between the two groups, determined by whether the data followed a normal distribution. Variance analysis or the Kruskal-Wallis test was employed for data comparison and analysis among multiple groups, contingent on the data variance homogeneity. A statistically significant difference between different groups led to pairwise comparisons using the Least-Significant Difference (LSD). A p-value less than 0.05 was considered statistically significant.

Results

LAMTOR1 inhibits exosomal PD-L1 secretion

Exosome, a type of extracellular vesicle (EV), contains bioactive proteins that impact both the tumor microenvironment (TME) and the immune system [23, 24]. In our research, exosomes from non-small cell lung cancer (NSCLC) cells were examined using transmission electron microscopy (TEM) (Fig. 1A) and nanoparticle tracking analysis (NTA) (Fig. 1B). Through western blot analysis, we assessed the expression levels of PD-L1 in various NSCLC cell lines. Our results revealed that PD-L1 expression was notably higher in the cell lines H460, H2009, HCC827, H1573, H820, H3122, Calu-1, H1975, and H358 compared to other cell lines (Fig. 1C). Subsequently, we employed enzyme-linked immunosorbent assay (ELISA) to measure the exosomal PD-L1 levels in a subset of NSCLC cell lines. Our findings highlighted a significant increase in exosomal PD-L1 release, particularly from the NSCLC cell lines H1975 and H358 (Fig. 1D). Exosomes were isolated using sucrose density gradient centrifugation, and the expression of PD-L1 within the exosomes was assessed via western blot analysis (Fig. 1E). LAMTOR1 plays a crucial role in lysosomal trafficking and degradation, particularly at late endosomes/lysosomes, where it serves as an anchor for the Ragulator complex [16–19]. Nevertheless, existing literature lacks insights into the influence of LAMTOR1 on released exosomal PD-L1. In order to clarify the correlation between the expression levels of LAMTOR1 and PD-L1, we quantified the expression levels of LAMTOR1 and PD-L1 in 85 NSCLC tissues using H-score (Histochemistry score). Through statistical analysis, we found a negative correlation between the expression levels of LAMTOR1 and PD-L1 in the 85 cases of NSCLC tissues (Fig. 1F, G). Additionally, we conducted a GST-pull down assay to elucidate the role of LAMTOR1. Mass spectrometry analysis demonstrated that LAMTOR1 regulates the lysosomal membrane and extracellular exosomes (Fig. 1H, I). Moreover, we found that LAMTOR1 inhibits the release of exosomal PD-L1 in NSCLC cells (Fig. 1J). Consequently, we explored whether LAMTOR1 hinders the function of $CD8^+$ T cells via exosomal PD-L1 (Fig. 1K). Exosomal PD-L1 derived from NSCLC cell lines that overexpress LAMTOR1 significantly enhanced the function of $CD8^+$ T cells. This was evidenced by an augmented proportion of cells with reduced CFSE dye intensity (%$CFSE^-$), elevated granzyme B (%$GzmB^+$) expression (Fig. 1L, M), and increased secretion of IFN-γ, IL-2, and TNF-α (Fig. 1N-Q). These findings suggest that LAMTOR1 suppresses exosomal PD-L1 to improve $CD8^+$ T cell function.

LAMTOR1 interacts with HRS inhibits exosomal PD-L1

Exosomes are generated and released via HRS-mediated recognition and sorting of exosome cargo [12]. Immunofluorescence imaging demonstrated the co-localization of PD-L1 with HRS in NSCLC cells (Fig. 2A). Subsequently, HRS was found to trigger the release of exosomal PD-L1 in NSCLC cells (Fig. 2B, C). Given that LAMTOR1 resides in late endosomes and lysosomes, and HRS is responsible for sorting exosome cargo, particularly PD-L1, we posited that LAMTOR1 may inhibit the secretion of exosomal PD-L1 regulated by HRS. Our western blot analysis supported this hypothesis by showing that LAMTOR1 suppresses HRS-mediated exosomal PD-L1 secretion (Fig. 2D). Furthermore, co-immunoprecipitation (Co-IP) experiments revealed the interaction between HRS and PD-L1 in NSCLC cells (Fig. 2E). Co-IP experiments also confirmed the association of LAMTOR1 with HRS and PD-L1 in NSCLC cells (Fig. 2F, G). Notably, upon deletion of HRS, the interaction between LAMTOR1 and PD-L1 was significantly diminished (Fig. 2H, I). These findings suggest that LAMTOR1 inhibits the HRS-regulated secretion of exosomal PD-L1.

LAMTOR1 inhibits exosomal PD-L1 by induced lysosomal degradation

To investigate whether LAMTOR1 suppresses exosomal PD-L1 secretion through the induction of the lysosomal degradation pathway [25]26, 27, we conducted experiments to test this hypothesis. We initially constructed and expressed a GFP-PD-L1 plasmid in NSCLC cells. Immunoblot analysis confirmed the expression of GFP-PD-L1 in both whole-cell lysates (WCL) and exosomes (EXO), as demonstrated in Fig. 3A, B. LAMTOR1 is known to regulate the lysosomal degradation of PD-L1 by recruiting it for degradation. Upon blocking lysosomes using the inhibitor Bafilomycin A1 (Baf-A1, which inhibits the fusion of autophagosomes with lysosomes, thereby suppressing acidification and protein degradation in lysosomes), we observed a significant increase in exosomal PD-L1 expression levels (Fig. 3C, D). This

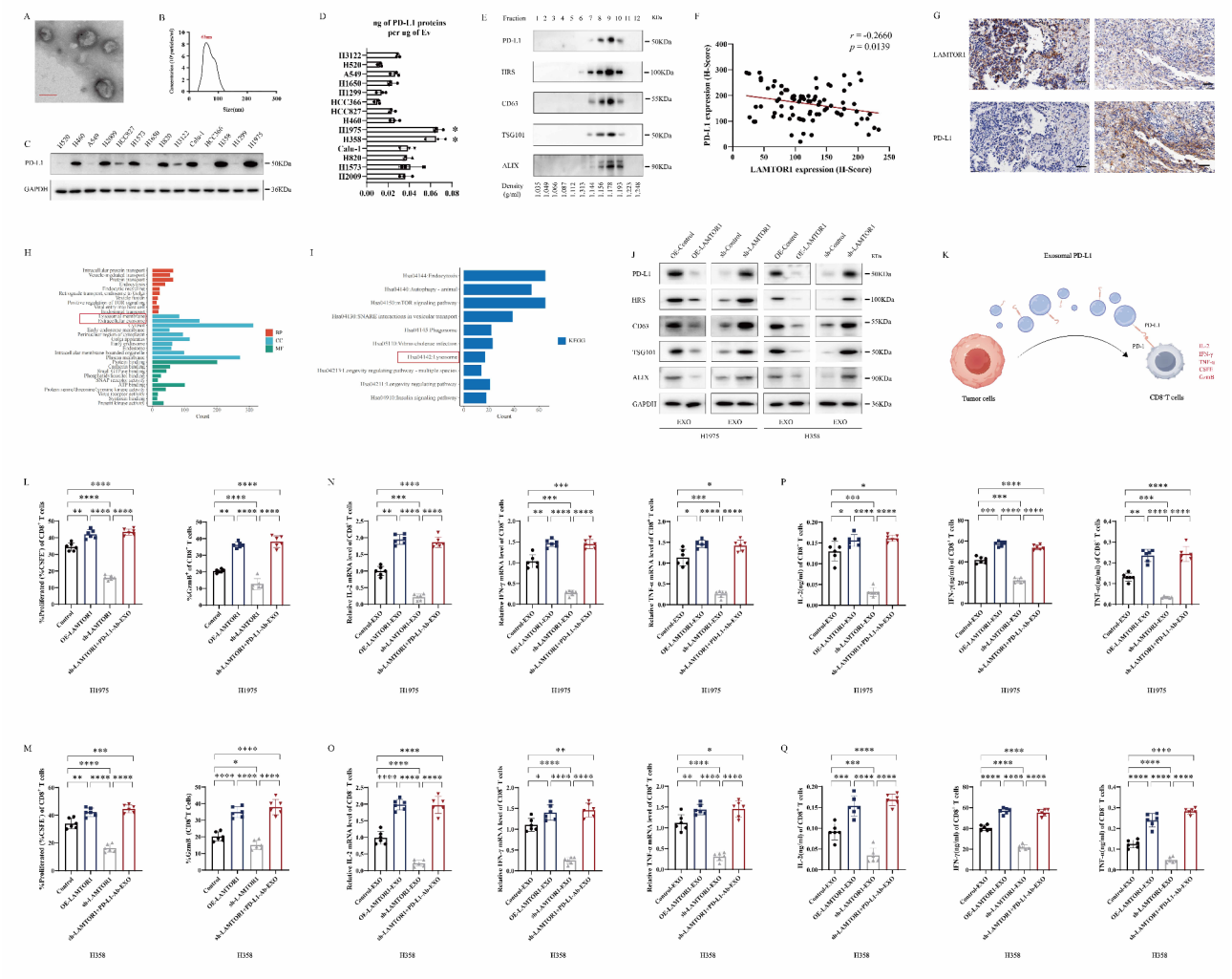

Fig. 1 LAMTOR1 inhibits exosomal PD-L1 secretion. (**A**, **B**) Transmission electron microscopy (TEM) and nanoparticle tracking analysis (NTA) were utilized to detect the release of exosomes from NSCLC cells. (**C**) Western blot analysis was performed to assess the expression of PD-L1 in whole-cell lysates (WCL). (**D**) ELISA was employed to detect the expression of PD-L1 on exosomes derived from NSCLC cells. (**E**) The density gradient centrifugation confirmed that NSCLC cells (H1975 and H358) secreted exosomal PD-L1, identified by the presence of HRS, CD63, TSG101, and ALIX. (**F**) The correlation between LAMTOR1 and PD-L1 expression levels in human NSCLC specimens was assessed using H-score (Histochemistry score). (**G**) The correlation between LAMTOR1 and PD-L1 expression levels in human NSCLC specimens was assessed using immunohistochemistry. Scale bars indicate 50 μm. (**H**, **I**) Construction of the GST-LAMTOR1 plasmid enabled the analysis of pathways and functions regulated by LAMTOR1 in NSCLC cells (H1975 and H358) using mass spectrometry. BP: biological process.; CC: cellular component; MF: molecular function; KEGG: Kyoto Encyclopedia of Genes and Genomes. (**J**) Western blot analysis was performed to investigate the regulation of exosomal PD-L1 by LAMTOR1 in NSCLC cells (H1975 and H358) treated with OE-LAMTOR1 or sh-LAMTOR1. (**K**) Exosomes collected from NSCLC cells (H1975 and H358) with OE-LAMTOR1 or sh-LAMTOR1 were co-cultured with $CD8^+$ T cells, and the functionality of $CD8^+$ T cells was assessed using RT-PCR, ELISA, and flow cytometry. (**L**, **M**) In addition, flow cytometry was utilized to evaluate the proliferation ($\%CFSE^-$) and cytotoxicity ($\%GzmB^+$) of $CD8^+$ T cells upon co-culturing with exosomes released from NSCLC cells (H1975 and H358) expressing different levels of LAMTOR1. When PD-L1 antibody blocking (10 μg/ml) was added to the co-culture system of $CD8^+$ T cells with exosomes isolated from sh-LAMTOR1 NSCLC cells (H1975 and H358), the proliferation and cytotoxicity functions of $CD8^+$ T cells were also evaluated. (**N**, **O**) The expression levels of IL-2, IFN-γ, and TNF-α in $CD8^+$ T cells were determined through RT-PCR upon co-culturing with exosomes from NSCLC cells (H1975 and H358) OE-LAMTOR1 or sh-LAMTOR1. When PD-L1 antibody blocking (10 μg/ml) was added to the co-culture system of $CD8^+$ T cells with exosomes isolated from sh-LAMTOR1 NSCLC cells (H1975 and H358), the expression levels of IL-2, IFN-γ, and TNF-α of $CD8^+$ T cells were also evaluated. (**P**, **Q**) Additionally, ELISA was used to measure the expression levels of IL-2, IFN-γ, and TNF-α in $CD8^+$ T cells treated with exosomes from NSCLC cells (H1975 and H358) overexpressing or underexpressing LAMTOR1. When PD-L1 antibody blocking (10 μg/ml) was added to the co-culture system of $CD8^+$ T cells with exosomes isolated from sh-LAMTOR1 NSCLC cells (H1975 and H358), the expression levels of IL-2, IFN-γ, and TNF-α of $CD8^+$ T cells were also evaluated. The results are presented as mean ± SEM from six assays, with statistical significance denoted as $^*P < 0.05$, $^{**}P < 0.01$, $^{***}P < 0.001$, $^{****}P < 0.0001$ based on Student's t test

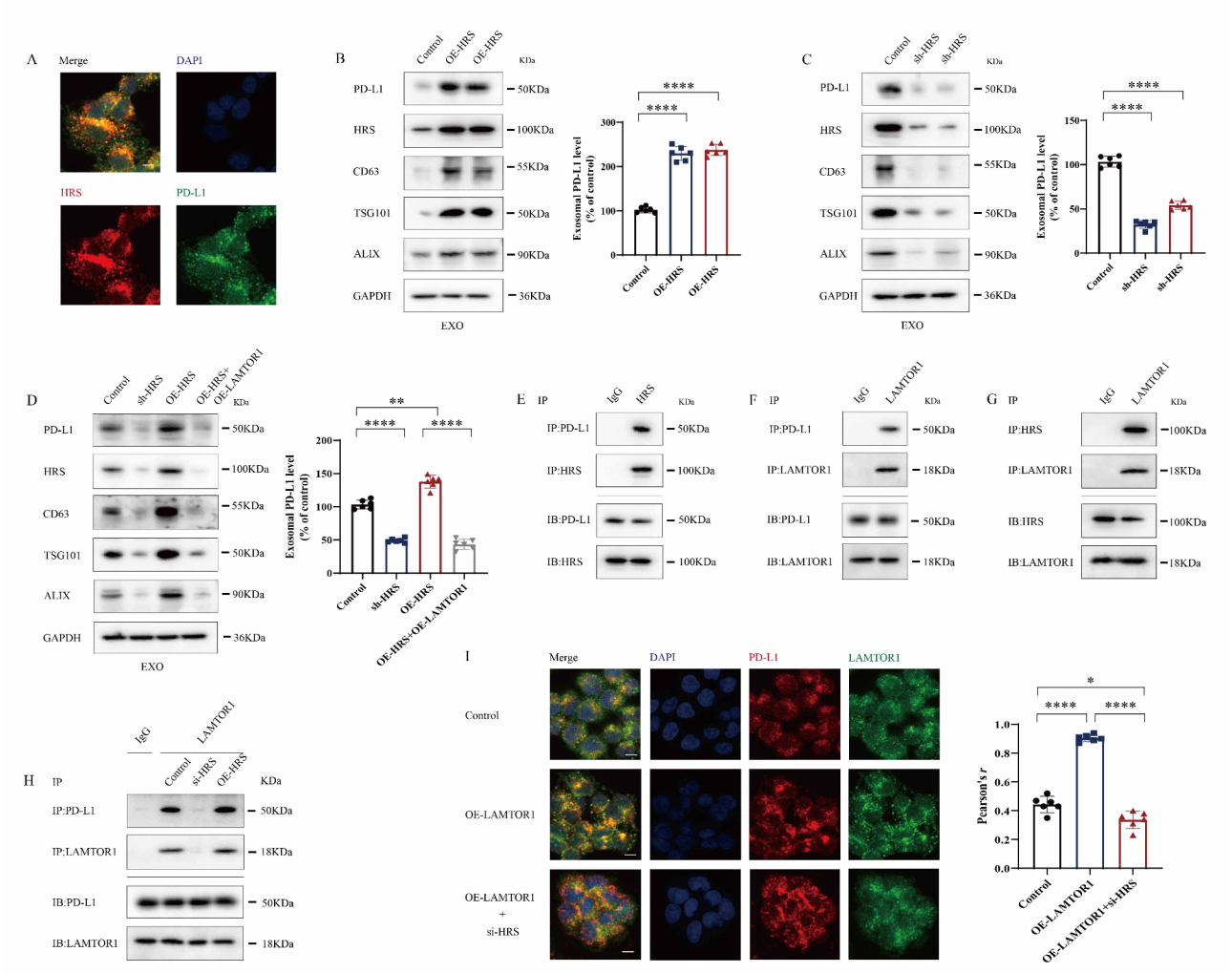

Fig. 2 The interaction between LAMTOR1 and HRS inhibits exosomal PD-L1. (**A**) Immunofluorescence demonstrates the co-localization of HRS and PD-L1 in non-small cell lung cancer (NSCLC) cells in NSCLC cells (H1975 and H358), with scale bars indicating 10 μm. (**B**, **C**) Western blot analysis was utilized to determine the expression levels of PD-L1 in exosomes (EXO) modulated by HRS. NSCLC cells in NSCLC cells (H1975 and H358) were subjected to OE-HRS or sh-HRS. The right graph quantifies the protein levels of exosomal PD-L1 from six independent experiments. (**D**) Additionally, western blotting was employed to evaluate the levels of PD-L1 in exosomes (EXO) influenced by HRS under the regulation of LAMTOR1. NSCLC cells in NSCLC cells (H1975 and H358) were treated with sh-HRS or OE-HRS in conjunction with OE-LAMTOR1. The right graph quantifies the protein levels of exosomal PD-L1 from six independent experiments. (**E**-**G**) Co-immunoprecipitation (Co-IP) assays were conducted to examine the interactions between HRS and PD-L1, LAMTOR1 and PD-L1, as well as LAMTOR1 and HRS in NSCLC cells (H1975 and H358). (**H**, **I**) Furthermore, Co-IP and immunofluorescence techniques were employed to validate that HRS regulates the interaction between LAMTOR1 and PD-L1 in NSCLC cells (H1975 and H358). The results are presented as mean ± SEM from six independent assays. Statistical significance was indicated by $^{*}P < 0.05$, $^{**}P < 0.01$, $^{***}P < 0.001$, $^{****}P < 0.0001$ based on Student's t-test

finding suggests that LAMTOR1 inhibits exosomal PD-L1 secretion by promoting lysosomal degradation. Immunofluorescence analysis demonstrated that LAMTOR1 facilitates the lysosomal degradation of PD-L1, as evidenced by the weakened interaction between LAMP1 and PD-L1 upon lysosome blockade (Fig. 3E). These results indicate that LAMTOR1 activates the PD-L1 lysosomal degradation pathway.

LAMTOR1 inhibits exosomal PD-L1 by induced autophagy-lysosomal degradation

Earlier studies have shown that the fusion of multivesicular bodies (MVBs) and autophagosomes can activate the lysosomal degradation pathway[26–28]. Transmission electron microscopy (TEM) images depicted that LAMTOR1 promoted the proliferation of MVBs and their fusion with lysosomes (Fig. 4A). Immunofluorescence analysis indicated that LAMTOR1 facilitated the fusion of MVBs (RAB7a) with autophagosomes (ATG7) (Fig. 4B). Previous research has demonstrated that RAB7a supports the fusion of endosomes-lysosomes

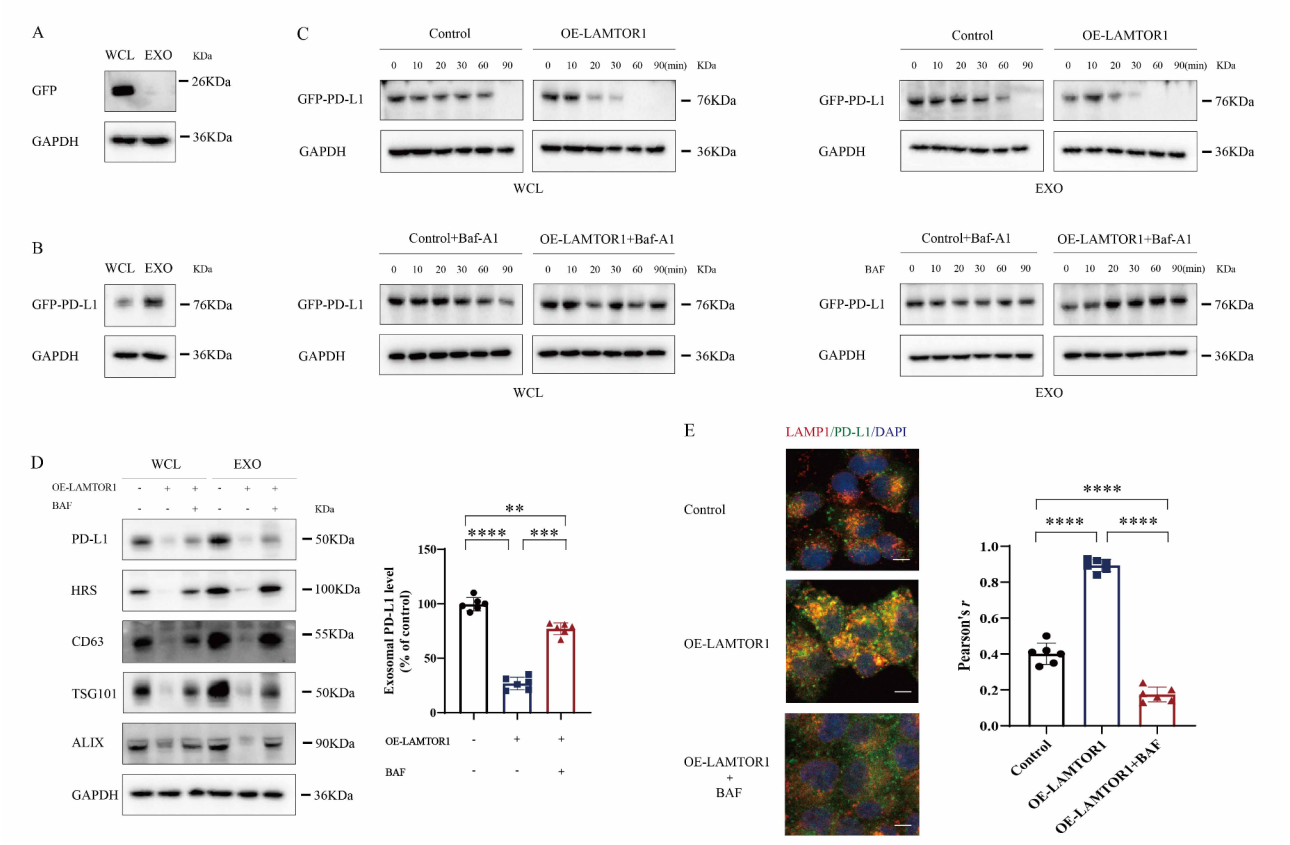

Fig. 3 LAMTOR1 induced lysosome degradation to inhibit exosomal PD-L1 secretion. (**A**, **B**) Transfect the GFP-PD-L1 plasmid into NSCLC cells (H1975 and H358) and employ western blot analysis to assess the PD-L1 expression in whole-cell lysates (WCL) and exosomes (EXO). (**C**) Furthermore, transfect NSCLC cells (H1975 and H358) with GFP-PD-L1 plasmid and conduct western blot analysis to investigate the upregulated LAMTOR1's impact on exosomal PD-L1 expression through the lysosomal degradation pathway. Subsequently, NSCLC cells (H1975 and H358) were treated with OE-LAMTOR1 in the presence or absence of 50 μM bafilomycin A1 (Baf-A1) treatment. (**D**) Western blot analysis to assess the PD-L1 expression in whole-cell lysates (WCL) and exosomes (EXO). Subsequently, NSCLC cells (H1975 and H358) were treated with OE-LAMTOR1 in the presence or absence of 50 μM bafilomycin A1 (Baf-A1) treatment. (**E**) Additionally, utilizing immunofluorescence staining, it was observed that LAMTOR1 facilitates the co-localization of PD-L1 with lysosomes (LAMP1). NSCLC Cells (H1975 and H358) were treated with OE-LAMTOR1 along with or without 50 μM bafilomycin A1 (Baf-A1). The scale bars indicate 10 μm. The results are presented as mean ± SEM from six independent experiments. Statistical significance was denoted as $^{*}P < 0.05$, $^{**}P < 0.01$, $^{***}P < 0.001$, $^{****}P < 0.0001$ based on Student's t-test

and autophagosomes-lysosomes. Through immunofluorescence, it was observed that the overexpression of LAMTOR1 promoted the colocalization of PD-L1 with lysosomes, whereas the colocalization of PD-L1 with lysosomes was diminished upon knockdown of RAB7a (Fig. 4C). Furthermore, immunoblot analysis revealed that upregulation of LAMTOR1 suppressed the secretion of exosomal PD-L1, which was restored upon RAB7a knockdown (Fig. 4D). Notably, when autophagy mediated by ATG7 was inhibited, the ability of LAMTOR1 to enhance the colocalization of PD-L1 with lysosomes was reduced, leading to the reversal of the inhibition of exosomal PD-L1 secretion (Fig. 4E, F), indicating the involvement of autophagy in the release of exosomal PD-L1. This discovery implicates that LAMTOR1-mediated fusion of MVBs and autophagosomes triggers PD-L1 lysosomal degradation.

LAMTOR1 interacts with HRS to regulate PD-L1 lysosomal degradation

Current research indicates that LAMTOR1 plays a crucial role in guiding lysosomal trafficking and degradation through its ubiquitination site [31]. Specifically, the N-terminal ubiquitination site located in the unstructured domain of LAMTOR1 facilitates autophagy [19]. To pinpoint the specific sites where LAMTOR1 regulates lysosomal function, the plasmid was constructed by deleting the ubiquitination residues K20, K31, and K60 in the N-terminal region. The immunofluorescent revealed that the N-terminal residues K20 and K31 are the key ubiquitin sites responsible for regulating lysosomal trafficking and degradation in LAMTOR1 (Fig. 5A). In addition, to investigate how LAMTOR1 modulates HRS activity, we transfected NSCLC cells with HA-HRS and GFP-LAMTOR1 to examine their association. Structural

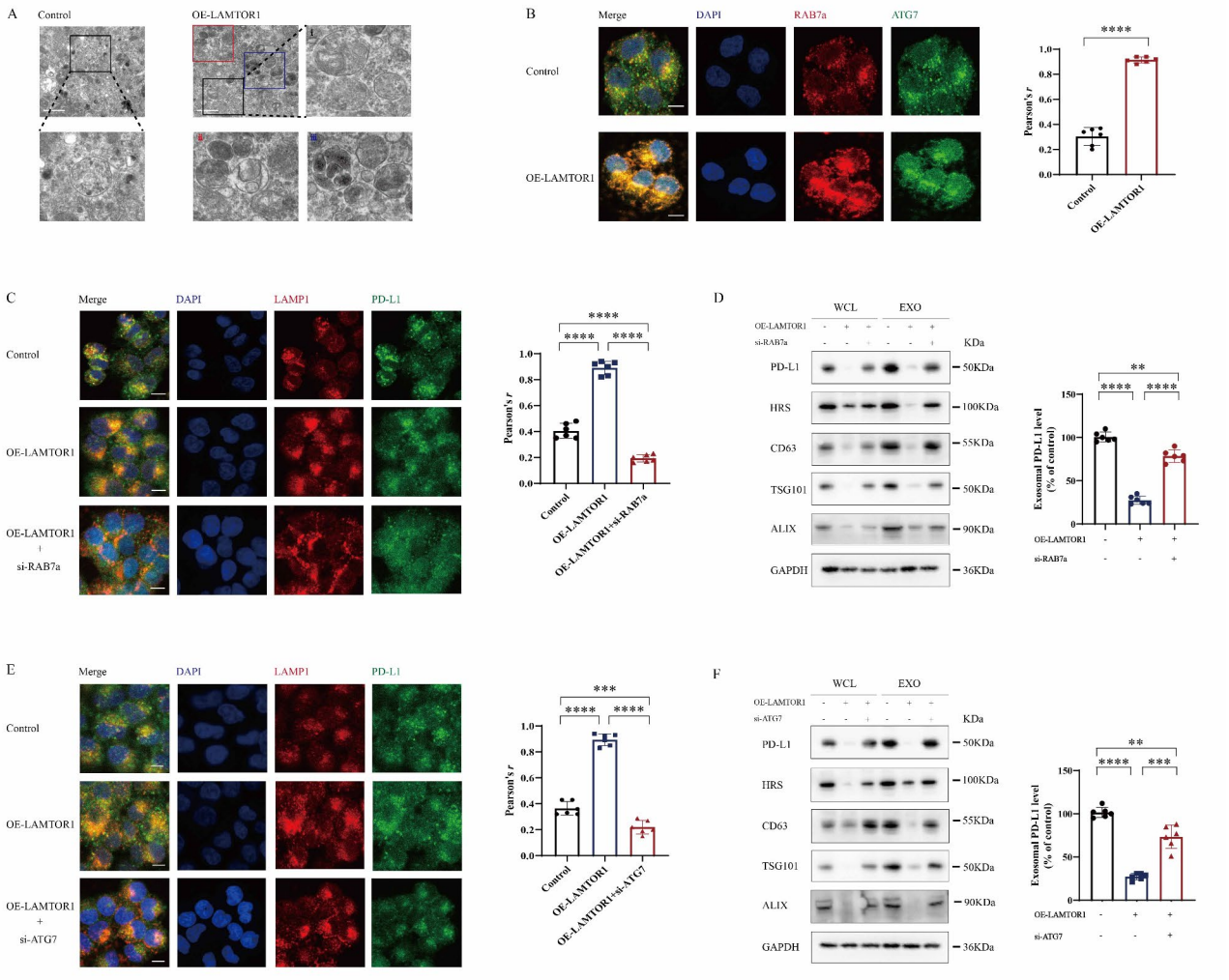

Fig. 4 LAMTOR1 inhibits exosomal PD-L1 by induced autophagy-lysosomal degradation. (**A**) Transmission electron microscopy (TEM) analysis revealed that LAMTOR1 facilitated an increase in the number of multivesicular bodies (MVBs) and their fusion with lysosomes in NSCLC cells (H1975 and H358). The scale bar in the insets is set at 500 nm. (**B**) Immunofluorescence studies demonstrated that LAMTOR1 induces the fusion of MVB (RAB7a) with autophagosome (ATG7) in NSCLC cells (H1975 and H358), with scale bars representing 10 μm. (**C**) Subsequently, NSCLC cells (H1975 and H358) co-transfected with OE-LAMTOR1 and si-RAB7a were assessed for the colocalization of PD-L1 with lysosomes (LAMP1), with scale bars representing 10 μm. (**D**) NSCLC cells (H1975 and H358) co-transfected with OE-LAMTOR1 and si-RAB7a were subjected to analysis of exosomal PD-L1 secretion through western blotting. NSCLC cells (H1975 and H358) were treated with OE-LAMTOR1 with or without si-RAB7a, and the right graph presents quantification of exosomal PD-L1 protein levels from six independent experiments. (**E**) Similar to previous setups, NSCLC cells (H1975 and H358) were treated with OE-LAMTOR1 with or without si-ATG7, and colocalization of PD-L1 with lysosomes (LAMP1) was evaluated. (**F**) Further experiments involved NSCLC cells (H1975 and H358) co-transfected with OE-LAMTOR1 and si-ATG7 for the analysis of exosomal PD-L1 secretion through western blotting. These results are represented as mean ± SEM from six assays, with significance levels indicated as follows: $^{*}P < 0.05$, $^{**}P < 0.01$, $^{***}P < 0.001$, $^{****}P < 0.0001$ based on Student's t test

analysis of Ragulator indicated that the middle region of LAMTOR1 is surrounded by LAMTOR2-LAMTOR3 and LAMTOR4-LAMTOR5, while the N-terminus (residues 1–19) directs LAMTOR1 to endosomes and lysosomes. Notably, the remaining LAMTOR1 N-terminal region (residues 20–78) and LAMTOR1 C-terminal region (residues 144–161) possess disordered and highly flexible features, including ubiquitination sites, indicating potential HRS interaction sites within these terminal regions. Subsequently, plasmids with deletions in either the N-terminal (residues ΔN1 (20–31), ΔN2 (31–60), ΔN3 (60–78)) or C-terminal (residues ΔC (144–161)) domains of LAMTOR1 were prepared (Fig. 5B). The co-IP analysis revealed that only the deletion of LAMTOR1 residues 20–30 significantly disrupted the LAMTOR1-HRS interaction (Fig. 5B). Further investigations utilizing constructs with LAMTOR1 N-terminal deletions (residues ΔN1-3 (20–78), ΔN1-2(20–60), ΔN1(20–31), ΔN2(31–60), ΔN3(60–78)) and LAMTOR1 C-terminal deletion (residues ΔC (144–161)) displayed that the deletion of LAMTOR1 residues 20–31 notably reduced the LAMTOR1-PD-L1 interaction (Fig. 5C-E).

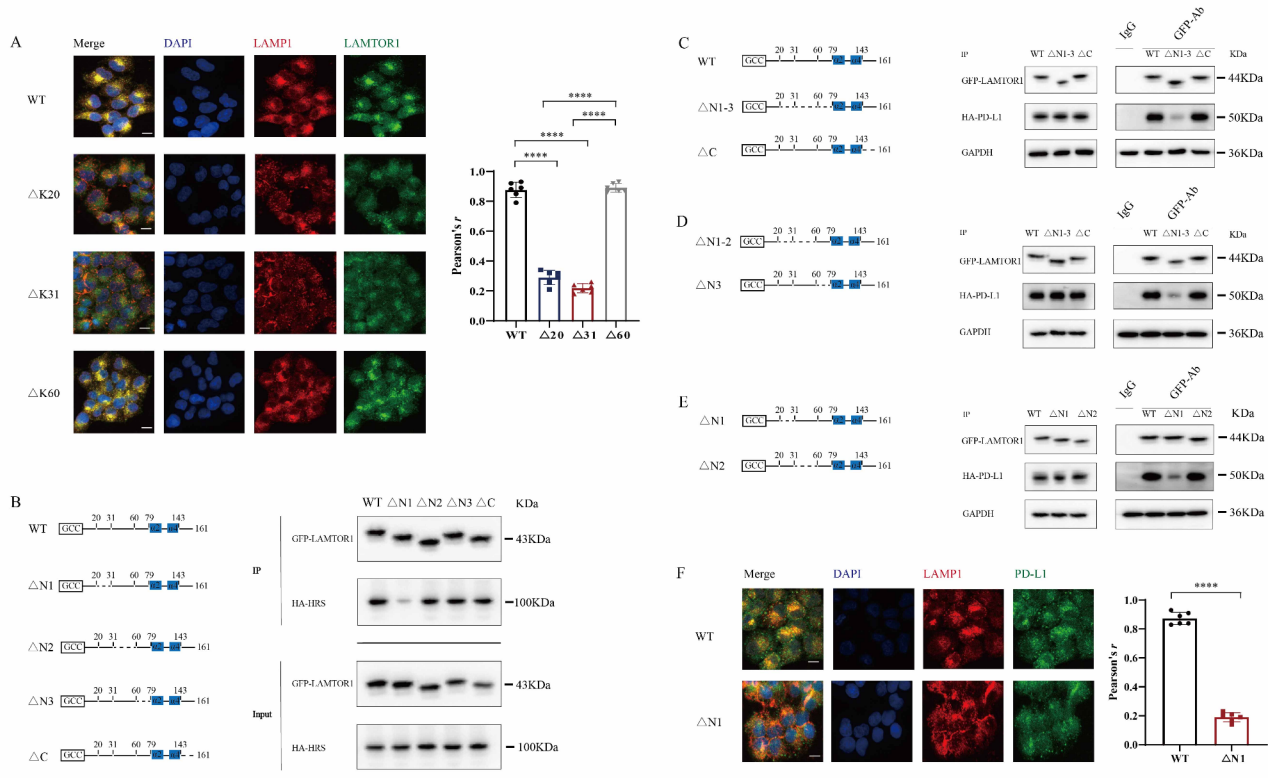

Fig. 5 LAMTOR1 interacts with HRS to regulate the lysosomal degradation of PD-L1. (**A**) Lysates from NSCLC cells (H1975 and H358) cotransfected with LAMTOR1 or its mutants (ΔK20, ΔK31, and ΔK60) were used for immunofluorescence to demonstrate the colocalization between LAMTOR1 and LAMP1, with scale bars representing 10 μm. (**B**) A schematic structure of LAMTOR1 is depicted with annotations indicating WT for wild-type, ΔN for N-terminal deletion, and ΔC for C-terminal deletion. The lysates from NSCLC cells (H1975 and H358) co-transfected with GFP-LAMTOR1 mutants (ΔN1, ΔN2, ΔN3, and ΔC) and HA-HRS showed co-IP of LAMTOR1 and HRS. (**C**-**E**) Additionally, lysates from NSCLC cells (H1975 and H358) cotransfected with GFP-LAMTOR1 or its mutants (ΔN1-3, ΔN1-2, ΔN1, ΔN2, ΔN3, and ΔC) and HA-PD-L1 were subjected to Co-IP of PD-L1 and LAMTOR1. (**F**) Furthermore, lysates from NSCLC cells (H1975 and H358) cotransfected with GFP-LAMTOR1 mutants (WT and ΔN1) were used to analyze the co-localization of LAMP1 and PD-L1 via immunofluorescence staining, with scale bars representing 10 μm. These results are represented as mean ± SEM from six assays, with significance levels indicated as follows: $^{*}P < 0.05$, $^{**}P < 0.01$, $^{***}P < 0.001$, $^{****}P < 0.0001$ based on Student's t test

Intriguingly, deletion of LAMTOR1 residues 20–31 also led to a significant decrease in the co-localization of PD-L1 with LAMP1 (Fig. 5F), suggesting that N-terminal residues 20–31 of LAMTOR1 are involved in the regulation of PD-L1 lysosomal degradation.

Rationally designed LAMTOR1 peptides target PD-L1 for lysosomal degradation

To investigate the functionality of the N-terminal region of LAMTOR1, we designed a GFP fusion protein and assessed its involvement in lysosomal degradation. Western blot analysis showed that the expression of GFP-S1 (LAMTOR1 (1–19, 20–31)) was lower compared to GFP-S2 (LAMTOR1 (1–19, 31–60)), GFP-S3 (LAMTOR1 (1–19, 60–78)), and GFP- (Fig. 6A). Our findings indicate that GFP-S1 is degraded, a process inhibited by the lysosomal inhibitor Baf-A1, suggesting that LAMTOR1 (1–31) mediates targeting for lysosomal degradation (Fig. 6B-D). Subsequently, we synthesized the LAMTOR1 peptide, LAMTOR1 peptide (1–31), which effectively reduced PD-L1 expression and promoted its degradation, an effect blocked by Baf-A1 (Fig. 6E-H). These results suggest that LAMTOR1 regulates PD-L1 through lysosomal degradation, and we further examined its impact on $CD8^+$ T cell activity in a co-culture system. Remarkably, the LAMTOR1 peptide significantly enhanced the function of $CD8^+$ T cells, including proliferation (%$CSFE^-$), cytotoxicity (%$GzmB^+$) (Fig. 6I) and cytokine production (IL-2, IFN-γ, and TNF-α) (Fig. 6J). The subsequent analysis evaluated the role of LAMTOR1 peptide in the potential treatment of lung tumors. Initially, lung tumors were induced in C57BL6 mice by intravenously injecting LCC cells into the tail vein. Since LCC cells do not express PD-L1, a LCC cell line overexpressing PD-L1 (LCC/PD-L1 cells) was engineered. Exosomes released by the PD-L1 overexpressing LCC cells were found to

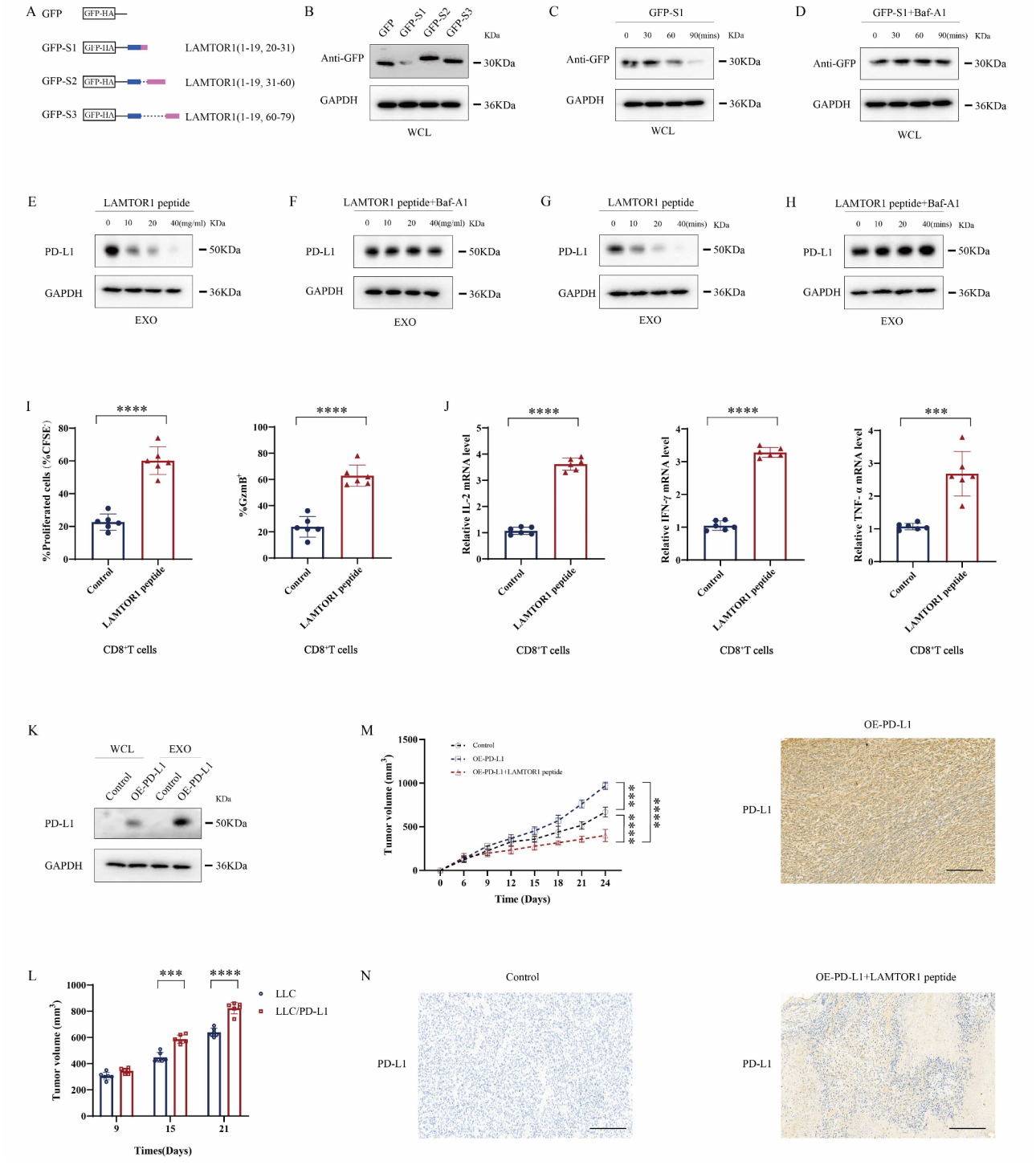

Fig. 6 (See legend on next page.)

contain PD-L1 (Fig. 6K). The construction of lung tumors in C57BL6 mice revealed that the overexpression of PD-L1 in LCC cells significantly promoted tumor growth (Fig. 6L). Furthermore, notable findings showed that during tumor formation, mice treated with either the control group or LAMTOR1 peptide every 3 days (Fig. 6M), which exhibited effective tumor growth inhibition by LAMTOR1 peptide. The study also examined the impact of LAMTOR1 peptide on the regulation of PD-L1 expression levels (Fig. 6N). The findings revealed a significant inhibitory effect of LAMTOR1 peptide on PD-L1 expression levels in lung tumors.

(See figure on previous page.)

Fig. 6 Rationally designed LAMTOR1 peptide targets PD-L1 to lysosomal degradation. (**A**) The study generated a GFP fusion protein based on LAMTOR1 sequences. (**B**-**D**) Western blot analysis identified the expression of different GFP fusion proteins (GFP-S1, GFP-S2, and GFP-S3) in NSCLC cells (H1975 and H358). Additionally, Western blot results showed that GFP-S1 underwent degradation, which was inhibited by treatment with Bafilomycin A1 (Baf-A1). (**E**-**H**) Furthermore, western blot analysis demonstrated that the degradation of exosomal PD-L1 could be prevented by Baf-A1 treatment. Subsequently, NSCLC cells (H1975 and H358) were exposed to the LAMTOR1 peptide with or without 50 μM Baf-A1 treatment. (**I**, **J**) In a separate experiment, NSCLC cells (H1975 and H358) co-cultured with LAMTOR1 peptide and $CD8^+$ T cells in Transwell chambers underwent analysis of $CD8^+$ T cell proliferation (%$CFSE^-$) and cytotoxic (%$GzmB^+$) function were evaluated through flow cytometry (**I**), while IL-2, IFN-γ, and TNF-α expression levels in $CD8^+$ T cells using RT-PCR (**J**). (**K**) Immunoblots were performed to assess exosomal PD-L1 levels in NSCLC cells (H1975 and H358) after PD-L1 overexpression. (**L**) The study also involved injecting C57BL6 mice ($n=6$/group) with LLC cells ($1\times10\text{^}6$) to generate subcutaneous tumors. After 21 days, the animals were euthanized, and tumor tissues were collected for volume analysis. (**M**) Moreover, C57BL6 mice ($n=10$/group) received injections of LLC/PD-L1 cells ($1\times10\text{^}6$) and were infected with either control or LAMTOR1 peptide on day 4. After 24 days, the animals were euthanized to collect tumor tissues for volume analysis. (**N**) The expression levels of PD-L1 in lung tumor was assessed using immunohistochemistry. Scale bars indicate 200 μm. The results are presented as mean ± SEM from six independent experiments, with statistical significance denoted by asterisks (*$P<0.05$, **$P<0.01$, ***$P<0.001$, ****$P<0.0001$) based on Student's t-test

Coadministration of LAMTOR1 peptide and anti-PD-1 immunotherapy for lung cancer

Our study has unveiled that the LAMTOR1 peptide facilitates the degradation of PD-L1 in lysosomes, leading to the suppression of exosomal PD-L1 release and thus, hindering the advancement of non-small cell lung cancer (NSCLC). PD-L1, a key immune cell surface protein that binds to the programmed cell death receptor 1 (PD-1), plays a pivotal role in enabling tumors to escape T cell-mediated immune responses. The interaction between PD-L1 and PD-1 can impede the effective functioning of T cells. Exosomes derived from tumor cells can transport PD-L1 to bind with PD-1 on $CD8^+$ T cells' surface, thereby compromising the cytotoxic capabilities of $CD8^+$ T cells and promoting tumor cells' immune evasion. As a result, we propose a dual therapeutic approach that combines the LAMTOR1 peptide with anti-PD-1 immunotherapy. In our study, we established an orthotopic lung cancer C57BL6 mouse model by intravenously injecting $1\times10\text{^}6$ LCC/PD-L1 cells via the tail vein. Starting on day 6, we administered LAMTOR1 peptide (50 mg/kg) and anti-PD-1 (200 μg) injections every three and six days, respectively, continuing until day 24. The control group, anti-PD-1 group, LAMTOR1 peptide group, and LAMTOR1 peptide+anti-PD-1 group received intravenous administrations accordingly (Fig. 7A). We employed the IVIS imaging system to evaluate the efficacy of this combined therapy, which showed a significant inhibition in mouse lung tumor growth (Fig. 7B, C). The inhibitory effect of the combined treatment of LAMTOR1 peptide and anti-PD-1 on lung tumor growth was subsequently validated (Fig. 7D, E). Immunohistochemistry results also show that the LAMTOR1 peptide significantly inhibits the expression levels of PD-L1 in lung tumors (Fig. 7F). Subsequent flow cytometry analysis of $CD8^+$ T cells in the treated lung tissue indicated that the combined treatment markedly enhanced $CD8^+$ T cell activity, as well as an augmented proportion of cells with reduced CFSE dye intensity (%$CFSE^-$), elevated granzyme B (%$GzmB^+$) expression (Fig. 7G). Consequently, the coadministration of LAMTOR1 peptide and anti-PD-1 significantly prolonged the survival of mice with lung cancer (Fig. 7H). Simultaneously employing H&E staining to investigate the potential detrimental effects of combining the LAMTOR1 peptide with immunotherapy, the study results suggest that the LAMTOR1 peptide predominantly induces harm in the lungs, liver and kidney (Fig. 7I). Consequently, the concurrent use of the LAMTOR1 peptide and anti-PD-1 therapy offers a hopeful therapeutic avenue for lung cancer, albeit requiring additional evaluation to appraise possible adverse reactions.

Discussion

Therapies utilizing immune checkpoint targets have demonstrated significant clinical benefits, and enriching checkpoint blockade efficiency necessitates a deeper comprehension of PD-L1 distribution changes within tumor microenvironment (TME) 35[36]. HRS, an ESCRT complex subunit, facilitates the identification and sorting of exosome cargo, internalizing PD-L1 into MVBs, and subsequently releasing through exosomes [12]. LAMTOR1 augments the lysosomal degradation of PD-L1 through its binding with HRS, which consequently prevents the exosomal release of PD-L1. Hence, LAMTOR1 markedly bolsters the production of cytokines, proliferation, and cytotoxicity in $CD8^+$ T cells by curtailing the release of exosomal PD-L1. We discerned in this study that LAMTOR1 improves anti-tumor immunity by suppressing exosomal PD-L1 release in NSCLC.

Restricting the autolysosome degradation pathway typically triggers exosome secretion, while enhanced autophagy or lysosomal function stimulates MVBs or amphisomes aimed at lysosomal degradation, mitigating exosome secretion to maintain cellular homeostasis [29, 30]. The LAMTOR1-mediated regulation of lysosomal degradation, a factor attributable to promoting endosome-lysosome and autophagosome-lysosome fusion pathways. The internalization of cargo proteins to MVBs or targeted lysosomal degradation by amphisome necessitates ESCRT complexes [37–40]. With its position on the late endosomal and lysosomal, LAMTOR1 emerges as a central hub for the regulation of intracellular

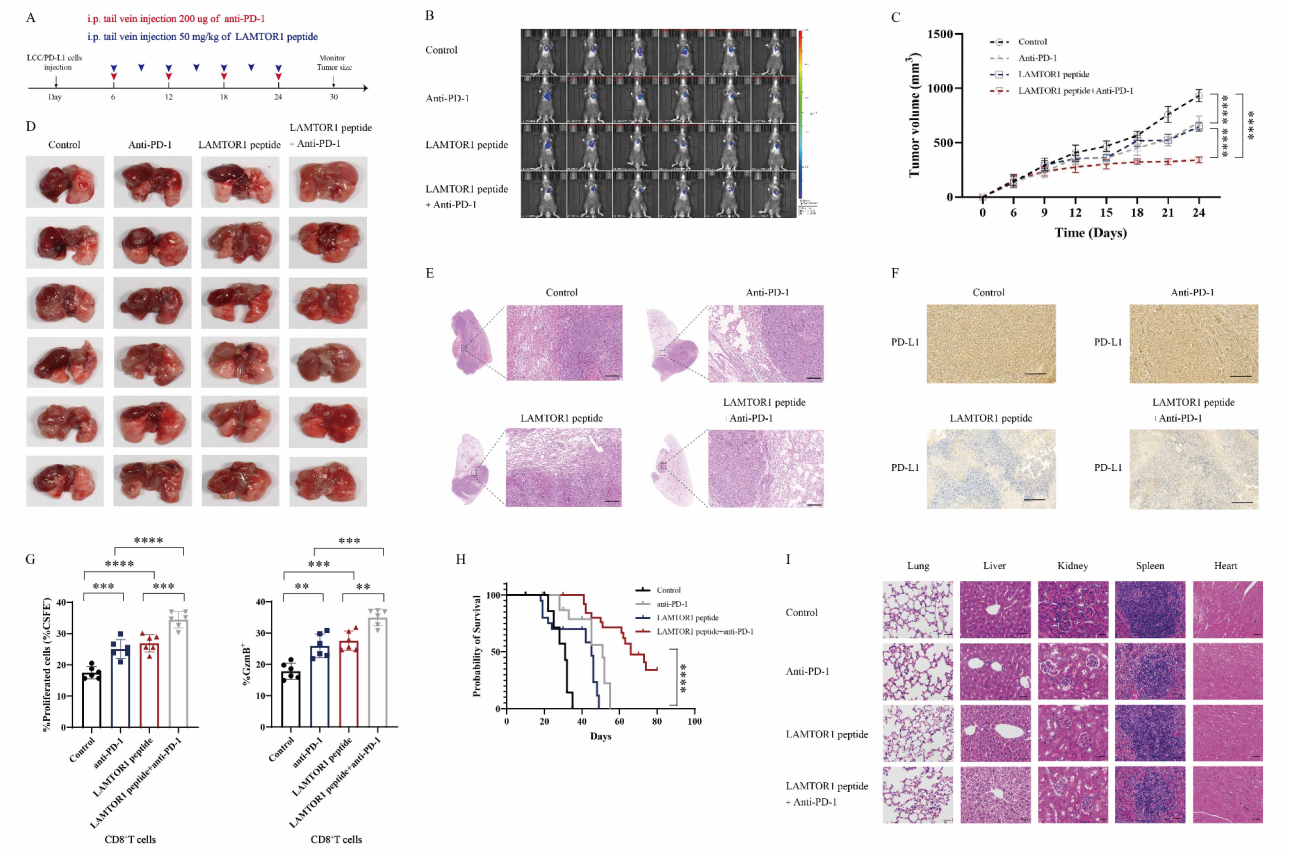

Fig. 7 LAMTOR1 peptide administration promotes anti-PD-1 therapy sensitivity in lung tumors. (**A**) The flowchart depicts the utilization of LAMTOR1 peptide and anti-PD-1 in the treatment of lung tumors. Starting from day 6, injections of LAMTOR1 peptide (50 mg/kg) and anti-PD-1 (200 μg) were administered every three and six days, respectively, until day 24. The injections were given via intravenous administration to the Control group, anti-PD-1 group, LAMTOR1 peptide group, and LAMTOR1 peptide + anti-PD-1 group. (**B**, **C**) Using the IVIS imaging system, it was observed that the combination of LAMTOR1 peptide and anti-PD-1 hindered the growth of lung tumors ($n = 6$/group). (**D**, **E**) Additionally, the inhibitory effect on lung tumor growth due to the combined treatment of LAMTOR1 peptide and anti-PD-1 was validated through HE staining, with scale bars representing 200 μm. (**F**) The expression levels of PD-L1 in lung tumors were evaluated through immunohistochemistry. The scale bars represent 200 μm. (**G**) Flow cytometry analysis indicated that the synergy between LAMTOR1 peptide and anti-PD-1 enhanced the activity of $CD8^+$ T cells, proliferation (%$CFSE^-$), and cytotoxicity (%$GzmB^+$). (**H**) The survival of mice within tumors ($n = 6$/group) was evaluated. (**I**) Examine the potential adverse effects of co-administering the LAMTOR1 peptide with immunotherapy, employing H&E staining to observe the treatment-induced damage to the lungs, liver, heart, kidney, and spleen, with scale bars representing 50 μm. The results are depicted as mean ± SEM from 3 assays, with statistical significance denoted as $^*P < 0.05$, $^{**}P < 0.01$, $^{***}P < 0.001$, $^{****}P < 0.0001$ based on 1-way ANOVA or log-rank test

signaling pathways [17]. The N-terminal ubiquitination site within the unstructured domain of LAMTOR1 facilitates autophagy [19]. Our findings suggest that LAMTOR1, via interaction with HRS and dependence on the ubiquitination site, manages intracellular positioning of PD-L1, promoting its lysosomal degradation. The focus of prospective cancer research, therefore, lies in developing novel lysosome targeted chimeras against immune checkpoint blockade.

Cancers cleverly circumvent immune surveillance, elevating PD-L1 expression [5] and understanding of PD-L1 promoted immune evasion is crucial in refining treatment outcomes [11–13]. Though PD-L1 is predominantly considered as cell membrane surface-bound, recent studies confirm its distribution in exosomes [41]. Current PD-L1 antibody successfully block cell surface PD-L1, but PD-L1 redistribution could diminish the potency of blocking antibodies [42]. Therefore, modifying combination therapy to control the dynamic spatial location of PD-L1 within cells could yield exceptional opportunities to overcome adaptive resistance to PD-L1 blockade [43]. Our study identifies the role of LAMTOR1 inhibited exosomal PD-L1 released, delivering novel insights into the mechanism that PD-L1 lysosomal degradation. The LAMTOR1 peptide rational design establishes a strategy to abate PD-L1 in exosomes using the lysosomal. These discoveries will advance and optimize the blueprint for degrading immune checkpoint targeting strategies. In our investigation, LAMTOR1 peptide effectively suppressed lung tumor growth in an experimental mouse model.

LAMTOR1 peptide also significantly enhanced the therapeutic efficacy of anti-PD-1. PD-L1/PD-1 interactions can limit T cell effector function [32–34]. LAMTOR1 peptide combined with anti-PD-1 immunotherapy promotes tumor infiltration of $CD8^+$ T cells, a prerequisite for a therapeutic response to TME. Therefore, this study illustrates the efficacy of LAMTOR1 peptide as a mode of NSCLC immunotherapy. The potential deleterious effects of combining LAMTOR1 peptide with immunotherapy were assessed using H&E staining. The study results indicated that LAMTOR1 peptide primarily caused damage to the lungs, liver and kidney. Peptide drugs occupy a structural niche between small molecules and proteins, providing distinct benefits of heightened specificity and reduced toxicity. Prior to their clinical utilization, it is imperative to assess their immunogenicity, safety pharmacology, genetic toxicity, developmental reproductive toxicity, phototoxicity, and carcinogenicity [44, 45]. Hence, building upon preliminary mechanistic investigations, a more in-depth evaluation and refinement of the LAMTOR1 peptide are essential to emphasize its specificity and safety in the management of NSCLC.

The revelation of LAMTOR1 regulated lysosomal degradation of PD-L1 presents a novel strategy for mitigating exosomal PD-L1, thereby reinforcing its relevance as a vital target for immunotherapy. While the study endorses the use of LAMTOR1 peptide as a therapeutic avenue, it fails to comprehensively examine potential side effects or toxicity issues. It is imperative that this area of research is thoroughly investigated prior to progressing to clinical trials. Moreover, considering that many tumors often develop mechanisms to resist treatment, a thorough understanding of these probable resistance pathways becomes crucial. Importantly, the study requires validation across an expanded range of experimental models, explicitly involving human specimens. Concurrently, elaborate studies investigating variances amongst different cancers are a prerequisite prior to asserting LAMTOR1 as a therapeutic target for other types of cancer.

Supplementary Information

The online version contains supplementary material available at https://doi.org/10.1186/s12943-024-02099-4.

Supplementary Material 1

Supplementary Material 2

Author contributions

B.W., L.Z., and HX.L. made equal contributions to this research. The study was conceived and designed by B.W., L.Z., and HX.L. B.W., X.H., X.S., and MX.J. carried out the experiments and developed the methodology. MX.J., X.S., and X.H. were responsible for collecting clinical samples. B.W. and L.Z. were involved in writing, reviewing, and revising the manuscript. B.W., L.Z., and HX.L. conducted data acquisition, analysis, interpretation, and statistical analysis. X.H., X.S., and MX.J. provided technical and material support. Funding acquisition and study supervision were managed by L.Z. and HX.L. All authors have reviewed and approved the final version of the manuscript.

Funding

This work was supported by the National Natural Science Foundation of China (No.82073286, No.82170047).

Data availability

No datasets were generated or analysed during the current study.

Declarations

Ethical approval

The studies involving animals adhered to the animal care regulations set forth by the Committee for Ethical Research Review at China Medical University and were conducted in accordance with the guidelines of the Institutional Animal Care and Use Committee (IACUC) under the reference number KT-20240394. Human NSCLC tissue samples were acquired with explicit written consent from patients or their legal representatives before their involvement in our research. The process of sample collection was sanctioned by the Ethics Review Committee at Liaoning Cancer Hospital & Institute, with the approval number KY20240337.

Competing interests

The authors declare no competing interests.

Received: 3 July 2024 / Accepted: 21 August 2024
Published online: 02 September 2024

References

1. Sun Q, Hong Z, Zhang C, Wang L, Han Z, Ma D. Immune checkpoint therapy for solid tumours: clinical dilemmas and future trends. Signal Transduct Target Ther. 2023;8:320. https://doi.org/10.1038/s41392-023-01522-4
2. Morad G, Helmink BA, Sharma P, Wargo JA. Hallmarks of response, resistance, and toxicity to immune checkpoint blockade. Cell. 2021;184:5309–37. https://doi.org/10.1016/j.cell.2021.09.020
3. Wang TW, Johmura Y, Suzuki N, Omori S, Migita T, Yamaguchi K, Hatakeyama S, Yamazaki S, Shimizu E, et al. Blocking PD-L1-PD-1 improves senescence surveillance and ageing phenotypes. Nature. 2022;611:358–64. https://doi.org/10.1038/s41586-022-05388-4
4. Cha JH, Chan LC, Li CW, Hsu JL, Hung MC. Mechanisms controlling PD-L1 expression in cancer. Mol Cell. 2019;76:359–70. https://doi.org/10.1016/j.molcel.2019.09.030
5. Sun C, Mezzadra R, Schumacher TN. Regulation and function of the PD-L1 checkpoint. Immunity. 2018;48:434–52. https://doi.org/10.1016/j.immuni.2018.03.014
6. Kjeldsen JW, Lorentzen CL, Martinenaite E, Ellebaek E, Donia M, Holmstroem RB, Klausen TW, Madsen CO, Ahmed SM, Weis-Banke SE, et al. A phase 1/2 trial of an immune-modulatory vaccine against IDO/PD-L1 in combination with nivolumab in metastatic melanoma. Nat Med. 2021;27:2212–23. https://doi.org/10.1038/s41591-021-01544-x
7. Patil NS, Nabet BY, Müller S, Koeppen H, Zou W, Giltnane J, Au-Yeung A, Srivats S, Cheng JH, Takahashi C, et al. Intratumoral plasma cells predict outcomes to PD-L1 blockade in non-small cell lung cancer. Cancer Cell. 2022;40:289–e3004.
8. Banchereau R, Leng N, Zill O, Sokol E, Liu G, Pavlick D, Maund S, Liu LF, Kadel E 3rd, Baldwin N, et al. Molecular determinants of response to PD-L1 blockade across tumor types. Nat Commun. 2021;12:3969. https://doi.org/10.1038/s41467-021-24112-w
9. Gao Y, Bi D, Xie R, Li M, Guo J, Liu H, Guo X, Fang J, Ding T, Zhu H, et al. Fusobacterium nucleatum enhances the efficacy of PD-L1 blockade in colorectal cancer. Signal Transduct Target Ther. 2021;6:398. https://doi.org/10.1038/s41392-021-00795-x
10. Chen G, Huang AC, Zhang W, Zhang G, Wu M, Xu W, Yu Z, Yang J, Wang B, Sun H, et al. Exosomal PD-L1 contributes to immunosuppression and is associated with anti-PD-1 response. Nature. 2018;560:382–6. https://doi.org/10.1038/s41586-018-0392-8
11. Lee YJ, Shin KJ, Jang HJ, Ryu JS, Lee CY, Yoon JH, Seo JK, Park S, Lee S, Je AR, et al. GPR143 controls ESCRT-dependent exosome biogenesis and promotes

cancer metastasis. Dev Cell. 2023;58:320–e3348. https://doi.org/10.1016/j.devcel.2023.01.006
12. Guan L, Wu B, Li T, Beer LA, Sharma G, Li M, Lee CN, Liu S, Yang C, Huang L, et al. HRS phosphorylation drives immunosuppressive exosome secretion and restricts CD8+T-cell infiltration into tumors. Nat Commun. 2022;13:4078. https://doi.org/10.1038/s41467-022-31713-6
13. de Araujo MEG, Naschberger A, Fürnrohr BG, Stasyk T, Dunzendorfer-Matt T, Lechner S, Welti S, Kremser L, Shivalingaiah G, Offterdinger M, et al. Crystal structure of the human lysosomal mTORC1 scaffold complex and its impact on signaling. Science. 2017;358:377–81. https://doi.org/10.1126/science.aao1583
14. Mu Z, Wang L, Deng W, Wang J, Wu G. Structural insight into the Ragulator complex which anchors mTORC1 to the lysosomal membrane. Cell Discov. 2017;3:17049. https://doi.org/10.1038/celldisc.2017.49
15. Yonehara R, Nada S, Nakai T, Nakai M, Kitamura A, Ogawa A, Nakatsumi H, Nakayama KI, Li S, Standley DM, et al. Structural basis for the assembly of the Ragulator-Rag GTPase complex. Nat Commun. 2017;8:1625. https://doi.org/10.1038/s41467-017-01762-3
16. Jia J, Abudu YP, Claude-Taupin A, Gu Y, Kumar S, Choi SW, Peters R, Mudd MH, Allers L, Salemi M, et al. Galectins control MTOR and AMPK in response to lysosomal damage to induce autophagy. Autophagy. 2019;15:169–71. https://doi.org/10.1080/15548627.2018.1505155
17. Nowosad A, Jeannot P, Callot C, Creff J, Perchey RT, Joffre C, Codogno P, Manenti S, Besson A. p27 controls ragulator and mTOR activity in amino acid-deprived cells to regulate the autophagy-lysosomal pathway and coordinate cell cycle and cell growth. Nat Cell Biol. 2020;22:1076–90. https://doi.org/10.1038/s41556-020-0554-4
18. Nakatani T, Tsujimoto K, Park J, Jo T, Kimura T, Hayama Y, Konaka H, Morita T, Kato Y, Nishide M, et al. The lysosomal Ragulator complex plays an essential role in leukocyte trafficking by activating myosin II. Nat Commun. 2021;12:3333. https://doi.org/10.1038/s41467-021-23654-3
19. Hertel A, Alves LM, Dutz H, Tascher G, Bonn F, Kaulich M, Dikic I, Eimer S, Steinberg F, Bremm A. USP32-regulated LAMTOR1 ubiquitination impacts mTORC1 activation and autophagy induction. Cell Rep. 2022;41:111653. https://doi.org/10.1016/j.celrep.2022.111653
20. Kim DH, Kim H, Choi YJ, Kim SY, Lee JE, Sung KJ, Sung YH, Pack CG, Jung MK, Han B, et al. Exosomal PD-L1 promotes tumor growth through immune escape in non-small cell lung cancer. Exp Mol Med. 2019;51:1–13. https://doi.org/10.1038/s12276-019-0295-2
21. D'Acunzo P, Kim Y, Ungania JM, Pérez-González R, Goulbourne CN, Levy E. Isolation of mitochondria-derived mitovesicles and subpopulations of microvesicles and exosomes from brain tissues. Nat Protoc. 2022;17:2517–49. https://doi.org/10.1038/s41596-022-00719-1
22. Wu B, Wang Q, Li B, Jiang M. LAMTOR1 degrades MHC-II via the endocytic in hepatocellular carcinoma. Carcinogenesis. 2022;43:1059–70. https://doi.org/10.1093/carcin/bgac075
23. Kalluri R, LeBleu VS. The biology, function, and biomedical applications of exosomes. Science. 2020;367:eaau6977. https://doi.org/10.1126/science.aau6977
24. Morrissey SM, Yan J. Exosomal PD-L1: roles in tumor progression and immunotherapy. Trends Cancer. 2020;6:550–8. https://doi.org/10.1016/j.trecan.2020.03.002
25. Hessvik NP, Llorente A. Current knowledge on exosome biogenesis and release. Cell Mol Life Sci. 2018;75:193–208. https://doi.org/10.1007/s00018-017-2595-9
26. Liu J, Ren L, Li S, Li W, Zheng X, Yang Y, Fu W, Yi J, Wang J, Du G. The biology, function, and applications of exosomes in cancer. Acta Pharm Sin B. 2021;11:2783–97. https://doi.org/10.1016/j.apsb.2021.01.001
27. Mathieu M, Névo N, Jouve M, Valenzuela JI, Maurin M, Verweij FJ, Palmulli R, Lankar D, Dingli F, Loew D, et al. Specificities of exosome versus small ectosome secretion revealed by live intracellular tracking of CD63 and CD9. Nat Commun. 2021;12:4389. https://doi.org/10.1038/s41467-021-24384-2
28. Villarroya-Beltri C, Baixauli F, Mittelbrunn M, Fernández-Delgado I, Torralba D, Moreno-Gonzalo O, Baldanta S, Enrich C, Guerra S, Sánchez-Madrid F. ISGylation controls exosome secretion by promoting lysosomal degradation of MVB proteins. Nat Commun. 2016;7:13588. https://doi.org/10.1038/ncomms13588
29. Tian X, Teng J, Chen J. New insights regarding SNARE proteins in autophagosome-lysosome fusion. Autophagy. 2021;17:2680–8. https://doi.org/10.1080/15548627.2020.1823124
30. Tan EHN, Tang BL. Rab7a and mitophagosome formation. Cells. 2019;8:224. https://doi.org/10.3390/cells8030224
31. Sun J, Liu Y, Hao X, Lin W, Su W, Chiang E, Baudry M, Bi X. LAMTOR1 inhibition of TRPML1-dependent lysosomal calcium release regulates dendritic lysosome trafficking and hippocampal neuronal function. EMBO J. 2022;41:e108119. https://doi.org/10.15252/embj.2021108119
32. D'Alise AM, Leoni G, De Lucia M, Langone F, Nocchi L, Tucci FG, Micarelli E, Cotugno G, Troise F, Garzia I, et al. Maximizing cancer therapy via complementary mechanisms of immune activation: PD-1 blockade, neoantigen vaccination, and Tregs depletion. J Immunother Cancer. 2021;9:e003480. https://doi.org/10.1136/jitc-2021-003480
33. Bhattacharjee A, Burr AHP, Overacre-Delgoffe AE, Tometich JT, Yang D, Huckestein BR, Linehan JL, Spencer SP, Hall JA, Harrison OJ, et al. Environmental enteric dysfunction induces regulatory T cells that inhibit local CD4+T cell responses and impair oral vaccine efficacy. Immunity. 2021;54:1745–e17577. https://doi.org/10.1016/j.immuni.2021.07.005
34. Dammeijer F, van Gulijk M, Mulder EE, Lukkes M, Klaase L, van den Bosch T, van Nimwegen M, Lau SP, Latupeirissa K, Schetters S, et al. The PD-1/PD-L1-checkpoint restrains T cell immunity in tumor-draining lymph nodes. Cancer Cell. 2020;38:685–e7008. https://doi.org/10.1016/j.ccell.2020.09.001
35. Wu M, Huang Q, Xie Y, Wu X, Ma H, Zhang Y, Xia Y. Improvement of the anticancer efficacy of PD-1/PD-L1 blockade via combination therapy and PD-L1 regulation. J Hematol Oncol. 2022;15:24. https://doi.org/10.1186/s13045-022-01242-2
36. Cristescu R, Mogg R, Ayers M, Albright A, Murphy E, Yearley J, Sher X, Liu XQ, Lu H, Nebozhyn M, et al. Pan-tumor genomic biomarkers for PD-1 checkpoint blockade-based immunotherapy. Science. 2018;362:eaar3593. https://doi.org/10.1126/science.aar3593
37. Henne WM, Buchkovich NJ, Emr SD. The ESCRT pathway. Dev Cell. 2011;21:77–91. https://doi.org/10.1016/j.devcel.2011.05.015
38. Babst M. MVB vesicle formation: ESCRT-dependent, ESCRT-independent and everything in between. Curr Opin Cell Biol. 2011;23:452–7. https://doi.org/10.1016/j.ceb.2011.04.008
39. McNally EK, Brett CL. The intralumenal fragment pathway mediates ESCRT-independent surface transporter down-regulation. Nat Commun. 2018;9:5358. https://doi.org/10.1038/s41467-018-07734-5
40. Tang S, Buchkovich NJ, Henne WM, Banjade S, Kim YJ, Emr SD. ESCRT-III activation by parallel action of ESCRT-I/II and ESCRT-0/Bro1 during MVB biogenesis. Elife. 2016;5:e15507. https://doi.org/10.7554/eLife.15507
41. Poggio M, Hu T, Pai CC, Chu B, Belair CD, Chang A, Montabana E, Lang UE, Fu Q, Fong L, et al. Suppression of exosomal PD-L1 induces systemic anti-tumor immunity and memory. Cell. 2019;177:414–e42713. https://doi.org/10.1016/j.cell.2019.02.016
42. Shen DD, Pang JR, Bi YP, Zhao LF, Li YR, Zhao LJ, Gao Y, Wang B, Wang N, Wei L, et al. LSD1 deletion decreases exosomal PD-L1 and restores T-cell response in gastric cancer. Mol Cancer. 2022;21:75. https://doi.org/10.1186/s12943-022-01557-1
43. Chen J, Lin Z, Liu L, Zhang R, Geng Y, Fan M, Zhu W, Lu M, Lu L, Jia H, et al. GOLM1 exacerbates CD8+T cell suppression in hepatocellular carcinoma by promoting exosomal PD-L1 transport into tumor-associated macrophages. Signal Transduct Target Ther. 2021;6:397. https://doi.org/10.1038/s41392-021-00784-0
44. Wang M, Liu J, Xia M, Yin L, Zhang L, Liu X, Cheng Y. Peptide-drug conjugates: a new paradigm for targeted cancer therapy. Eur J Med Chem. 2024;265:116119. https://doi.org/10.1016/j.ejmech.2023.116119
45. Wang J, Chen L, Qin S, Xie M, Luo SZ, Li W. Advances in biosynthesis of peptide drugs: technology and industrialization. Biotechnol J. 2024;19:e2300256. https://doi.org/10.1002/biot.202300256

Publisher's note